



Article

*Present address: JEOL Ltd., 1-2 Musashino, 3-Chome Akishima, Tokyo 196-8558, Japan.

Cite this article: Uchida T, Shigeyama W, Oyabu I, Goto-Azuma K, Nakazawa F, Homma T, Kawamura K, Dahl-Jensen D (2022).

Discovery of argon in air-hydrate crystals in a deep ice core using scanning electron microscopy and energy-dispersive X-ray spectroscopy. *Journal of Glaciology* **68**(269), 547–556. <https://doi.org/10.1017/jog.2021.115>

Received: 4 August 2021

Revised: 11 October 2021

Accepted: 12 October 2021

First published online: 18 November 2021

Key words:

Air hydrate; argon; energy-dispersive X-ray spectroscopy; NEEM ice core; scanning electron microscopy

Author for correspondence:

Tsutomu Uchida,

E-mail: t-uchida@eng.hokudai.ac.jp

Discovery of argon in air-hydrate crystals in a deep ice core using scanning electron microscopy and energy-dispersive X-ray spectroscopy

Tsutomu Uchida¹ , Wataru Shigeyama^{2,3,*}, Ikumi Oyabu³, Kumiko Goto-Azuma^{2,3}, Fumio Nakazawa^{2,3}, Tomoyuki Homma⁴, Kenji Kawamura^{2,3,5}  and Dorthe Dahl-Jensen⁶ 

¹Faculty of Engineering, Hokkaido University, N13 W8 Kita-ku, Sapporo 060-8628, Japan; ²The Graduate University for Advance Studies, SOKENDAI, 10-3 Midori-cho, Tachikawa, Tokyo 190-8518, Japan; ³National Institute of Polar Research, 10-3 Midori-cho, Tachikawa, Tokyo 190-8518, Japan; ⁴Nagaoka University of Technology, 1603-1 Kamitomioka-machi, Nagaoka 940-2188, Japan; ⁵Japan Agency for Marine Science and Technology (JAMSTEC), 2-15 Natsushima-cho, Yokosuka 237-0061, Japan and ⁶Centre for Ice and Climate, Niels Bohr Institute, University of Copenhagen, Juliane Maries Vej 30, 2100 Copenhagen K, Denmark

Abstract

Tiny samples of ancient atmosphere in air bubbles within ice cores contain argon (Ar), which can be used to reconstruct past temperature changes. At a sufficient depth, the air bubbles are compressed by the overburden pressure under low temperature and transform into air-hydrate crystals. While the oxygen (O₂) and nitrogen (N₂) molecules have indeed been identified in the air-hydrate crystals with Raman spectroscopy, direct observational knowledge of the distribution of Ar at depth within ice sheet and its enclathration has been lacking. In this study, we applied scanning electron microscopy (SEM) and energy-dispersive X-ray spectroscopy (EDS) to five air-hydrate crystals in the Greenland NEEM ice core, finding them to contain Ar and N. Given that Ar cannot be detected by Raman spectroscopy, the method commonly used for O₂ and N₂, the SEM-EDS measurement method may become increasingly useful for measuring inert gases in deep ice cores.

1. Introduction

The pores in snow contain atmospheric air that transforms to preserved-air bubbles when the pores close off. These air bubbles in an ice core are the only known paleoenvironmental archive of the actual ancient atmosphere with a time axis in the depth direction. For the orbital dating of ice cores, the composition ratio of oxygen (O₂) to nitrogen (N₂) is useful because it correlates with fluctuations in local summer insolation (e.g. Bender, 2002; Kawamura and others, 2007; Suwa and Bender, 2008a, b; Landais and others, 2012; Bazin and others, 2013, 2016). In particular, summer insolation may influence certain physical properties of snow that control the magnitude of close-off fractionation (Bender, 2002; Kawamura and others, 2007; Fujita and others, 2009).

Greenhouse gases such as carbon dioxide (CO₂) and methane (CH₄) are trace components in the atmosphere, and their past atmospheric concentrations can only be known from the analysis of deep ice cores. Their concentrations correlate strongly with past global climate, so they are an important part of the ice-core analysis (e.g. Barnola and others, 1988; Kobashi and others, 2007; Chappellaz and others, 2013). Analyses of noble gases such as argon (Ar), krypton (Kr), and xenon (Xe) have been attracting attention because their elemental and isotopic ratios can be used to reconstruct various environmental parameters such as the temperature changes in the firn or ocean (e.g. Severinghaus and others, 1998; Severinghaus, 1999; Kobashi and others, 2008a, b, 2015; Orsi and others, 2014, 2017; Bereiter and others., 2018). Also, the ⁴⁰Ar/³⁸Ar ratio can be used for dating very old ice, based on the increasing rate of atmospheric ⁴⁰Ar over a million-year timescale (Bender and others, 2008).

As they descend deeper, the loading pressure causes the air bubbles to shrink. Below a certain depth, the temperature and pressure are sufficient for them to transform to air-hydrate crystals. During this phase change, the molecule with the lower dissociation pressure at the same temperature is enclathrated at a higher concentration than that in the original air in the bubble. In the ice sheet, the guest fractionation in air-hydrate crystals is enhanced by the different permeation rates of air molecules (N₂, O₂, Ar, ...) in the ice matrix (Ikeda and others, 1999; Ikeda-Fukazawa and others, 2001; Salamatin and others, 2001, 2003). For example, of the N₂ and O₂ components, the O₂ concentration becomes higher in the air-hydrate crystals than that in bubbles in the bubble-to-air hydrate transition zone (BHTZ), which has been identified by Raman spectroscopy as the change of the peak intensity ratio between O₂ and N₂ (Nakahara and others, 1988; Ikeda and others, 1999; Ikeda-Fukazawa and others, 2001). This bubble-air hydrate fractionation effect would be caused by the dissociation pressure of O₂ hydrate is lower than that of N₂ hydrate (about 6.5 MPa vs 9 MPa at –20 °C, Miller, 1969) and the

© The Author(s), 2021. Published by Cambridge University Press. This is an Open Access article, distributed under the terms of the Creative Commons Attribution licence (<https://creativecommons.org/licenses/by/4.0/>), which permits unrestricted re-use, distribution, and reproduction in any medium, provided the original work is properly cited.

[cambridge.org/jog](https://www.cambridge.org/jog)

permeation effect of O₂ in ice matrix is larger than that of N₂ (Salamatin and others, 2001; Ikeda-Fukazawa and others, 2005; Oyabu and others, *in review*, 2021).

Argon forms a gas hydrate with a dissociation pressure of about 5 MPa at −20°C (Nagashima, and others, 2018), which is below those of N₂ and O₂ hydrates (Fig. 1). Thus, Ar might be selectively enclathrated into air-hydrate crystals. In addition, as N₂, O₂, and Ar all form the type II crystal structure of clathrate hydrates (Davidson, and others, 1984; Hondoh and others, 1990), these gases can be enclathrated in the same type of crystal structure.

Atmospheric components in ice cores are usually measured by extracting all air from the ice by either melting or by physically destroying the bulk ice core sample (100 g or less). Concerning Ar, detailed analyses of firn air and ice cores have found Ar subject to size-dependent and mass-dependent fractionation during the close-off and post-coring gas loss (Bender and others, 1995; Huber and others, 2006; Severinghaus and Battle, 2006; Severinghaus and others, 2009; Kobashi and others, 2015; Oyabu and others, *in review*, 2021). At depths below the bubble–air-hydrate transition zone, Ar is considered to be included in air-hydrate crystals, but has yet to be confirmed directly by microscopic analysis. Such direct observation of Ar is difficult because it has a very small mixing ratio. Moreover, Ar is an inert gas, which makes it difficult to measure by the common spectroscopic methods used for N₂ and O₂. Also, little is known about the movement of Ar in the ice matrix, with only a few published simulations (Ikeda-Fukazawa and others, 2004; Kobashi and others, 2015) and experiments (e.g. Satoh and others, 1996). By identifying the presence and dynamics of Ar in the ice sheet, the accuracy of ice-core analysis should be further improved.

Here, we examine sections of the ice core retrieved at NEEM, Greenland, applying scanning electron microscopy (SEM) to five air-hydrate crystals in the deep ice. By analyzing the Ar signal from energy-dispersive X-ray spectroscopy (EDS) of the air-hydrate crystals, we argue that Ar exists in the air-hydrate crystals of deep ice cores.

Based on our discovery, we will be able to analyze the gas distribution in ice sheets. For example, the data on N₂/O₂ fractionation in the transition zone obtained with Raman spectra measurements (Ikeda and others, 1999; Ikeda-Fukazawa and others, 2001) were used to constrain mathematical models describing the formation and growth of air-hydrate crystals in ice sheets and to estimate the permeation coefficients of N₂ and O₂ molecules in ice (Salamatin and others, 2001, 2003), later on these estimates of permeation coefficients were used to simulate the diffusive smoothing of the delta O₂/N₂ orbital signal in old ice (e.g. Oyabu and others, *in review*, 2021). Knowledge of permeation coefficients (including that of Ar) is also important for assessing the selective gas loss from ice cores after coring (e.g. Ikeda-Fukazawa and others, 2005; Oyabu and others, 2020). Experimental data on the Ar/N₂ ratio may help to extend the existing models of bubble-to-hydrate transformation and of diffusive mass transport of air constituents through the ice matrix. The isotopic measurements would also be available by some microscopic methods in the future.

2. Methods

2.1 NEEM ice core

The Greenland NEEM ice core was extracted at 77.45 °N, 51.06 °W, at an altitude of 2450 m above sea level. The location has an annual mean temperature of −29°C with an annual mean surface mass-balance of 0.22 m in ice equivalent. The NEEM project (2008–2012) drilled to bedrock at a depth of 2537 m, with the

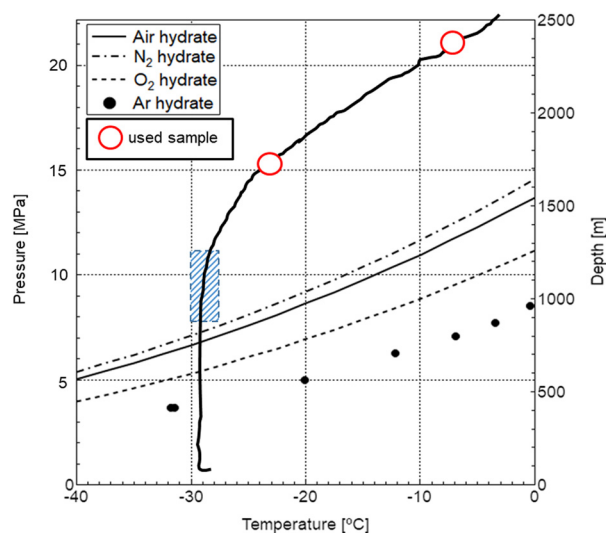


Fig. 1. Dissociation curves of air hydrates (left ordinate) and temperature-depth profile at the NEEM site (right ordinate, matched to left). Red circles are the depths of the samples used here, the blue rectangle is the estimated bubble-hydrate transition zone (BHTZ). The N₂, O₂, and air hydrate data are from Miller (1969). The Ar hydrate data are from Nagashima and others (2018). NEEM D data are from Sheldon and others (2014).

resulting extracted ice going back about 130 000 years (NEEM comm. members, 2013).

Until present, no detailed investigation has been conducted on air-hydrate crystals in NEEM ice cores. Considering the bore-hole temperature profile (Sheldon and others, 2014), the phase equilibrium condition of air-hydrate crystal (Miller, 1969), and the air-hydrate distributions analyzed in various deep cores (Uchida and others, 2014), the BHTZ should occur from about 850 to 1250 m (rectangular box in Fig. 1). It has been reported that the brittle zone in this core is from 600 to 1250 m, particularly in 750–1100 m (Rasmussen and others, 2013), where the mechanical properties of the core samples are weakened. As the brittle zone and the transition zone are known to be in good agreement (Uchida and others, 1994a), we consider that the prediction of the transition zone in Figure 1 would be valid.

Here we analyze ice-core samples from two depths: 1548 m (last glacial period, about 19.2 ka BP) and 2406 m (last interglacial period, about 125.5 ka BP). These ages of the core samples were derived from Rasmussen and others (2013). As these depths are well below the transition zone, the air inclusions in these ice cores immediately after retrieval should be only air-hydrate crystals.

The 1548 m core was drilled in 2009, the 2406 m core in 2010. Both were kept at about −20 to −25°C during the drilling operation and transportation. After arriving in Japan, they were stored in a low-temperature room at −50°C at the National Institute of Polar Research (NIPR) for about 8 years.

2.2 SEM sample preparation

We followed essentially the same experimental procedures as Shigeyama and others (2019), so here we describe them only briefly.

From the ice core stored at −50°C, we cut out a thin-section sample (about 10–20 mm × 10 mm × 1–4 mm) with a band saw in a low-temperature room at −20°C. The ice sample was set to the SEM holder (consisting of a shuttle and an aluminum stub) with a frozen adhesive (Tissue Tek, Sakura Finetek Japan) that includes polyvinyl alcohol and polyethylene glycol (safety data sheet, Tissue Tek). Then, the surface of the ice sample was flattened with a microtome. The air inclusions were observed and

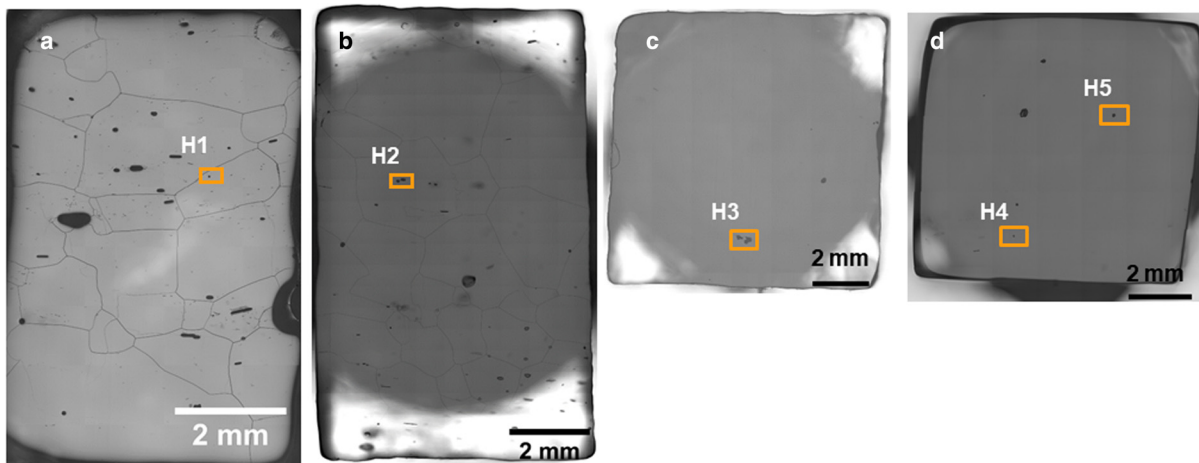


Fig. 2. Thin section samples with locations of the analyzed air-hydrate crystals in the sample. (a) From the 1548 m ice core (2815-C-IV-1). Box shows air-hydrate H1. (b) Air hydrate H2 from the 1548 m ice core (2815-D-I-1). (c) Air hydrate H3 from the 2406 m ice core (4375-A-V-1). (d) Air hydrate H4 and H5 from the 2406 m ice core (4375-B-II-2). The core numbers are the same as those described in another study (Shigeyama and others, 2021).

check their locations in the sample by an optical microscope (BX 51; Olympus Corporation, Tokyo, Japan) to analyze the same air-hydrate crystal by SEM/EDS. These processes lasted more than 5 h during which the sample was kept at -20°C .

For transferring the sample to the SEM preparation chamber (-190°C), we used liquid N_2 to keep the sample cold to avoid further ice relaxation and frost condensation. Then, the sample was installed on the cold stage (-140°C) in the SEM sample chamber (120 Pa of N_2 gas atmosphere). To eliminate surface frost, and to smooth the sample surface, the sample was sublimed by increasing the temperature of the cold stage to about -80°C for about 5 min before the observations.

2.3 SEM observations and EDS measurements on air-hydrate crystals

For the SEM observations, we used an environmental SEM (Quanta 450 FEG; Thermo Fisher Scientific) equipped with a cryogenic preparation system (PP3010; Quorum Technologies, Lewes, UK). The EDS measurements used an energy-dispersive X-ray spectrometer (X-Max 50; Oxford Instruments, plc, Abingdon, UK) with an acceleration voltage of 20 kV. To reduce buildup of surface charge, N_2 gas was purged and observations were made in low vacuum mode (120 Pa). An EDS measurement of a single spot was integrated until the X-ray count reached 3×10^6 (about 1 min). To ignore the damage of the sample due to the EDS measurement, multiple measurements were carried out on different points for an air-hydrate crystal.

The EDS's energy resolution is about 10 eV. We estimated the spatial resolution of the EDS measurements by comparing measurements across an air-hydrate crystal to the surrounding ice crystal, finding a value of about $15 \mu\text{m}$, which is much smaller than the roughly $100 \mu\text{m}$ diameter size of the air-hydrate crystals.

Thin-section images showing the two air-hydrate crystals (labeled H1 and H2) from the 1548 m depth, and the three air-hydrate crystals (H3, H4, and H5) from the 2406 m depth are shown in Figure 2.

3. Results and discussion

3.1 Optical microscope observations and SEM images of air-hydrate crystals

The optical microscopic observations revealed several types of air inclusions, specifically air-hydrate crystals, air bubbles, and plate-

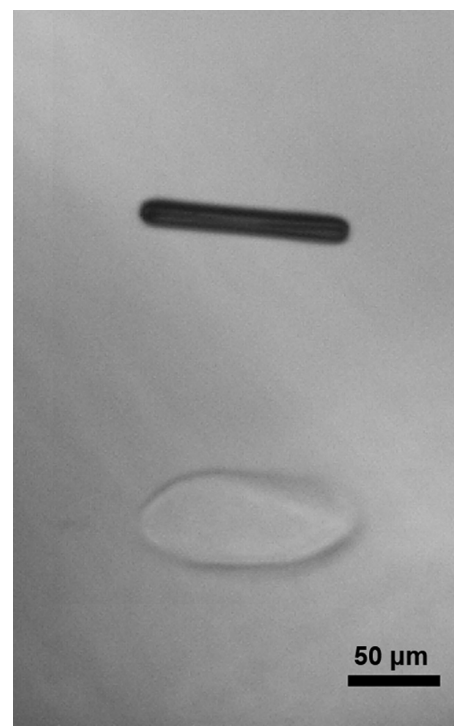


Fig. 3. Typical air inclusions in the 1548 m NEM ice core were observed by an optical microscope. A plate-like inclusion (top), a transparent air-hydrate crystal (bottom).

like inclusions (PLI; Fig. 3). Since the observed ice core samples were from depths below BHTZ (Fig. 1), air inclusions other than air-hydrate crystals were formed after the ice core recovery. Thus, we briefly consider how the transport and storage may have affected the hydrate crystal. After recovery, the ice core was kept at about -20 to -30°C for about 1 year at the drilling site to its transportation to Japan, and then kept at -50°C in the storage room for about 8 years until our analysis. At atmospheric pressure and -50°C , almost no air-hydrate crystals dissociate (Uchida and others, 1994b), indicating that the bubbles and PLIs observed in the present study likely formed during transport and storage, or during the thin-section sample preparation. However, the microscope images showed that many air-hydrate crystals had not dissociated. We conclude that the storage and handling conditions of the samples used in the present study were sufficient for the purpose of this study.

During the SEM-EDS measurements, cross-sections of the air-hydrate crystals are exposed to the low pressure (120 Pa N₂) condition under low temperature (−140°C) in the SEM sample chamber. So, we briefly consider their stability on the SEM's stage. Air-hydrates are thermodynamically unstable under the condition of −140°C and 120 Pa N₂ atmosphere, yet the dissociation rate at sub-zero temperatures is suppressed by the self-preservation effect (Uchida and others, 2011). Moreover, the dissociation rate of gas hydrates can be reduced by keeping the SEM's stage temperature low, a method that has enabled SEM observations of CH₄ hydrates (Stern and others, 2004), CO₂ hydrates (Kuhs and others, 2004), and air hydrates (Barnes and others, 2002). From these considerations, the SEM observations here should accurately show the hydrate crystals as they were in the deep ice.

The SEM images in Figure 4 show fine structures inside the air-hydrate crystals. The source of this structure is unclear, but is similar to the structure seen in the 'globular-type air-hydrate' from the GRIP ice core (Barnes and others, 2002). To confirm that the observation targets were air-hydrate, we observed the crystals during multi-step sublimation. Figure 5 shows the changes in observation target H5 at each step. Figure 5 (i), shows the upper-half cross-section of H5. After three sublimation steps, the size and shape of the newly exposed cross-section change as shown in Figure 5 (ii). The internal pattern has also changed, with the fine structure in Figure 5 (i) becoming coarser in Figure 5 (ii). With further sublimation steps, the outer shape and internal pattern change further (Fig. 5 (iii)–(iv)). These observations show H5 to be clearly different from the surrounding ice, with changes occurring during sublimation. For an object of this size to exist in the ice core, it would have to be an air-hydrate crystal. Therefore, we conclude that H5, as well as the similar cases H1–H4, are air-hydrate crystals.

NEEM ice-core samples are known to have particles of salt and other compounds (e.g. Oyabu, 2015; Oyabu and others, 2015; Eichler and others, 2017; Schüpbach and others, 2018). These particles contain Si, Fe, Na, Mg, Al, S, K, and Ca, with some particles attached to bubbles (Shigeyama and others, 2021). Using the following line of reasoning, we selected air-hydrate crystals that clearly contained fine particles on its surface or inside. First, the particle can act as a nucleus for promoting the phase change from bubble to air-hydrate crystal (Ohno and others, 2010). Therefore, the air-hydrate crystal with a particle would likely have formed relatively early (i.e. at a shallower depth) in the transition zone. Then, considering the fractionation effect, we expect that such an air-hydrate crystal would enclathrate more Ar in the crystal. Although the air components would be changed to the original one below BHTZ (Oyabu and others, *in review*, 2021), we chose higher possibility conditions that were likely to find Ar in the air-hydrate crystals.

3.2 EDS measurements of air-hydrate crystals

In examining the EDS results, we start by focusing on hydrate H3 (Fig. 4). Figure 6a shows the position of the air-hydrate crystal with an optical microscope. The part of the crystal viewed with a SEM secondary electron image is in Figure 6b. The higher magnification image in Figure 6c shows the positions of the EDS measurements on ice outside the air-hydrate (white '+') and on the inside of the air-hydrate crystal (yellow '*').

The EDS spectrum of ice in Figure 7a shows a large O peak at 0.53 keV, derived from H₂O, plus smaller peaks for C at 0.28 keV, from the background (likely from the freeze adhesive), and N at 0.39 keV, derived from the chamber gas. There is also a weak, broad background peak at 1–8 keV. In contrast, the spectrum from the inside of the air-hydrate crystal (Fig. 7b) shows a

much stronger N peak intensity and a weak, yet distinct, Ar peak at about 2.95 keV.

For the ice case, we attribute the N peak to the chamber gas because we observed a similar N peak in the spectrum of pure ice in a comparative measurement (Fig. S1). We also found that signals from various substances used in the sample holder and SEM chamber (Fig. S2) do not appear in Figure 7. These tests help confirm that the EDS spectra in Figure 7 come from ice, air-hydrate, and chamber gas, not the sample holder.

To remove the signal that is not from the sample and to extract the characteristic signals of the air-hydrate crystal, we subtracted an average ice spectrum from the spectrum from an air-hydrate crystal. This average ice spectrum comes from averaging the EDS spectra from several points surrounding the air-hydrate crystal (e.g. the white '+' in Fig. 6c). The resulting difference spectrum for H3 is shown in Figure 8. The difference spectrum of H3 shows both N and Ar peaks as positive values, whereas the O peak is negative. As both spectra are from nearby positions, they should both have the same contribution of N from the atmosphere of the SEM chamber. Thus, the N signal in the difference should largely be from the air-hydrate crystal. By this argument, the three peaks in Figure 8 are considered to be from elements in the air-hydrate crystal: N₂, O₂, and Ar. This appears to be the first time that experiment has shown an air-hydrate crystal in an ice core to contain Ar.

If the air-hydrate crystal contains Ar at the current atmosphere proportion (0.93%), the intensity of Ar signal would be near the noise level of this sample or close to the sensitivity limit in the EDS measurement. We had chosen only air-hydrate crystals with particles to possibly increase the Ar signal, but it is difficult to estimate the intensity quantitatively. Thus, the difference-spectrum analysis method should be useful for Ar observation in the air-hydrate crystal. Concerning the composition ratio, we did not calculate this ratio from the peak intensity because we did not run an EDS measurement on a standard sample. So, the concentration of each component in the air-hydrate crystal cannot be discussed here.

Concerning the reason for a negative O peak, we argue as follows. The O elements producing the peak are H₂O molecules in both the ice and air-hydrate crystals, plus the enclathrated guest molecule O₂ in the air-hydrate. (Although we don't know the accurate value of O₂ dissolved in the ice matrix, we consider it to be negligible small comparing to the sensitivity limit in the EDS measurement.) Assuming that ice is a pure ice single crystal (0.917 g cm^{−3}), the number concentration of O surrounding the air-hydrate crystal is the concentration of H₂O molecules in ice:

$$6.02 \times 10^{23} [\text{mol}^{-1}] / (18.015 [\text{gmol}^{-1}] / 0.917 [\text{gcm}^{-3}]) \\ \sim 3.06 \times 10^{22} [\text{cm}^{-3}]. \quad (1)$$

In the air-hydrate crystal, the number concentration of O equals the concentration of host H₂O molecules constructing the single crystal of structure-II hydrate plus twice that of the guest O₂ molecules. We estimate the total number in a unit cell by assuming the occupancy ratio of a guest molecule to be 0.9 (Hondoh and others, 1990) and the fraction of O₂ in guest molecules to be that in the normal atmosphere. Specifically, for the latter fraction, we use 0.2 because the ice-core samples are from depths below the transition zone (e.g. Ikeda-Fukazawa and others, 2001). Finally, we divide by the unit-cell volume to get

$$(136 [\text{host H}_2\text{O}] + 24 \times 0.9 \times 0.2 [\text{guest O}_2] \times 2) / (1.7 \\ \times 10^{-7} [\text{cm}])^3 \\ \sim 2.94 \times 10^{22} [\text{cm}^{-3}] \quad (2)$$

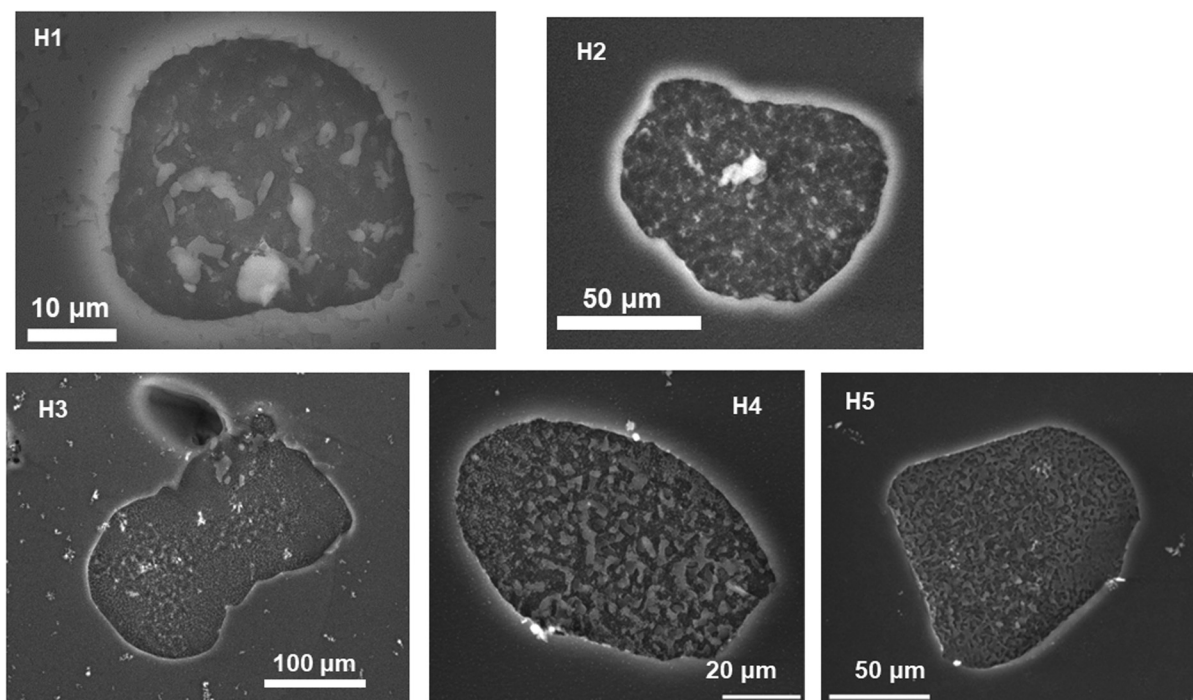


Fig. 4. SEM images of air-hydrate crystals used for the EDS measurements.

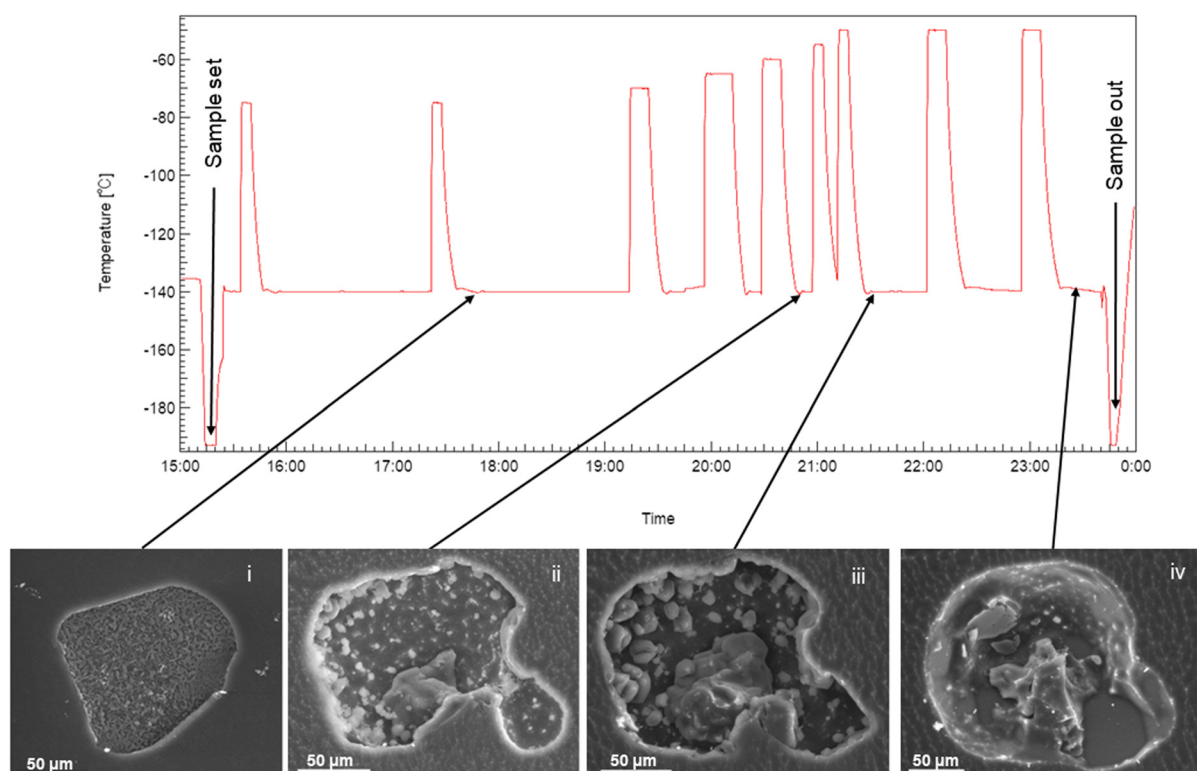


Fig. 5. Temperature–time series of air-hydrate H5 on the SEM cold stage showing multiple sublimation steps (top) and SEM images of the crystal (bottom).

where the denominator on the left side is the unit-cell volume. As this concentration is less than that of the pure ice, the intensity of O in the air-hydrate crystal should be less than that of pure ice making the peak intensity of O negative in the difference spectrum.

The EDS spectra at multiple points in all five air-hydrate crystals (two from 1548 m and three from 2406 m) indicated the existence of N, O, and Ar elements. Given the small signal-to-noise

ratio (S/N) of the Ar peak from each spectrum, we added all Ar signals from both air-hydrate crystals H1 and H2 in the 1548 m sample to make one spectrum. The same was done for air-hydrate crystals H3 and H4 in the 2406 m sample and shown in Figure 9. The Gaussian fit (Origin 2021, Lightstone) gives a weak yet distinct signal-to-noise ratio of about 3 and peak energy of 2.964 (3) keV (the error being the fit's standard deviation.). This peak energy coincides well with the characteristic X-ray line of Ar,

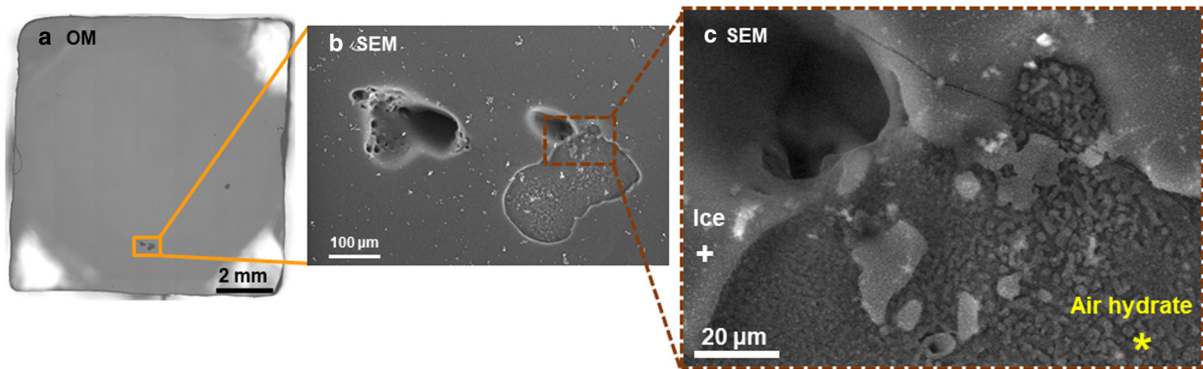


Fig. 6. Sample images of air-hydrate crystal H3 from the 2406 m ice core. (a) Optical microscope image of the thin section (same as Fig. 2 (c)). (b) SEM image. The object on the left side is the hollow of a dissociated air-hydrate crystal due either to the surface cutting or by the primary sublimations. (c) Expanded SEM image of the upper part of air-hydrate (H3) sample. The white '+' is the EDS measurement position in the ice, the yellow '*' that for the air-hydrate crystal.

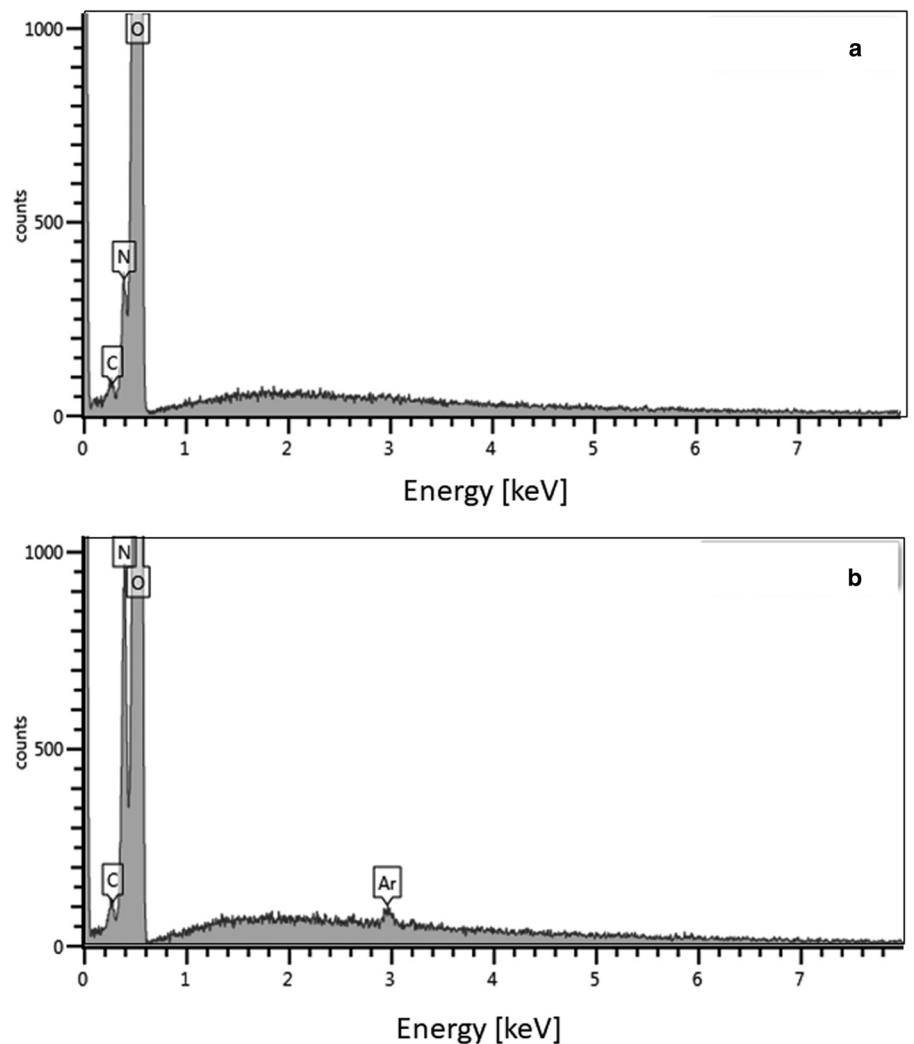


Fig. 7. EDS spectra (0–8 keV) obtained from the two points shown in Figure 6c. (a) Ice. (b) Air-hydrate crystal.

$K\alpha$ at 2.958 keV (Goldstein and others, 2003) within the energy resolution of the EDS measurement (approximately 10 eV). Another element that has a characteristic X-ray line in this energy region is silver (Ag: $L\alpha = 2.984$ keV (Goldstein, and others, 2003)), but an Ag signal was not observed in the EDS measurement of the SEM holder (see Fig. S2) nor in the fine particles. The analysis thus confirms that this peak is Ar in the air-hydrate crystal.

We ran the same analysis on both the N and O spectra, with the results of the gaussian fitting summarized in Table 1. The analyses indicate that all peaks could be identified with the literature values, and that the difference between the ice-core samples taken from different depths was within the error range.

As another test of the source of the N signal in the air-hydrate spectra, we ran the EDS measurements at several steps during the sublimation of hydrate H5. The peak for N in Figure 10

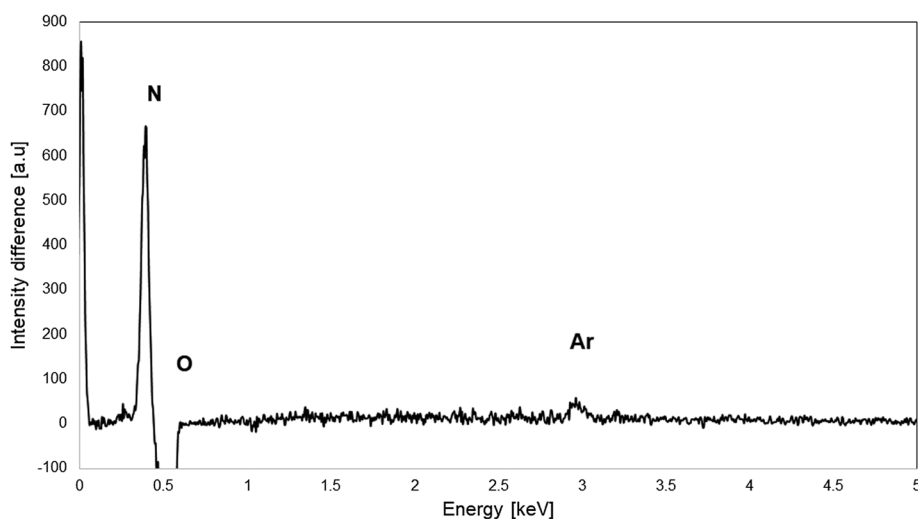


Fig. 8. Differential spectrum of air-hydrate crystal (from data in Fig. 7).

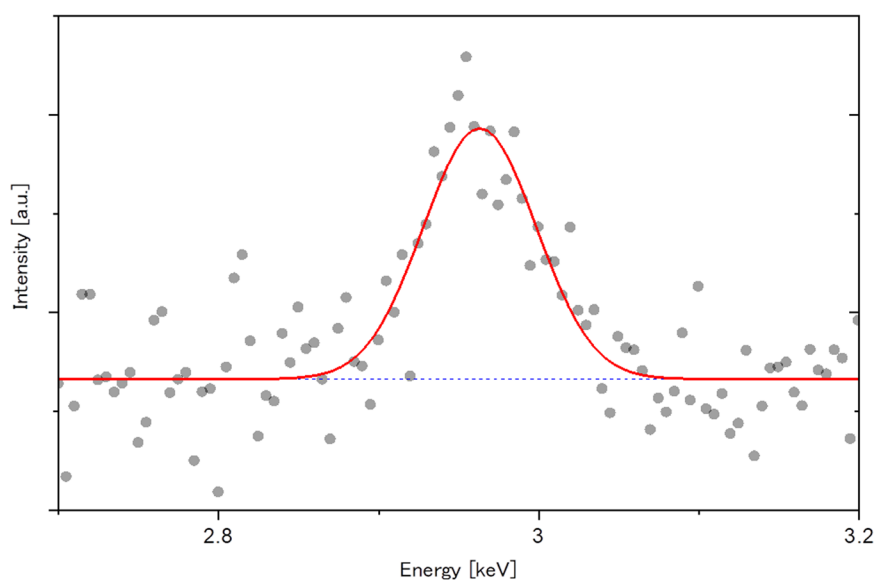


Fig. 9. Differential spectrum from Ar in 2406 m sample from the combination of 13 spectra. Solid circles are data points, red solid line is the Gaussian fitting curve ($R^2 = 0.73$), and the blue dashed line is the fitted base line.

continuously decays after each sublimation step. For example, several curves included in the group of (i) in Figure 10 were obtained between when SEM images (i) and (ii) were obtained, in which three sublimation steps were operated (Fig. 5). Note that the spectra obtained between sublimation processes were reproducible (for example, spectra with the highest peak). Therefore, an air-hydrate crystal was dissociated not by an EDS measurement, but by the sublimation process in our experimental conditions. By the sublimation step imaged as (iii), the N peak has vanished. Thus, as the N peak vanished with the inner fine structure, the EDS measurements suggest that the measured N (as well as the Ar) signals came from the guest molecules in the air-hydrate crystal.

We also ran SEM-EDS measurements on the fine particles associated with these five air-hydrate crystals. In the resulting EDS spectra, we frequently observed that the signals from the particle overlapped those from the neighboring air-hydrate crystal (for detailed data, see Shigeyama and others, 2021). Therefore, it is difficult to confirm whether the constituent elements of the fine particles contain those with a peak near 3 keV. However, when the hydrate H5 sample was sublimated until the N peak vanished, the EDS measurement of the fine particles attached to the hydrate showed no peaks near 3 keV. Consistent with this finding, previous SEM-EDS analyses of 838 particles from

Table 1. EDS peak fittings of Ar, N, and O in air-hydrate crystals.

		Average [keV]	S.D. [keV]	n
Ar	1548 m	2.968	0.009	3
($K\alpha_1$: 2.958 keV)	2406 m	2.964	0.003	13
N	1548 m	0.386	0.001	4
($K\alpha_1$: 0.392 keV)	2406 m	0.387	0.001	11
O	1548 m	0.520	0.002	4
($K\alpha_1$: 0.525 keV)	2406 m	0.521	0.001	11

(Reference values in parentheses are the characteristic X-ray lines from Goldstein and others, 2003).

1550.7 and 2401.6 m depths in the NEEM ice core showed almost no particles with a peak near 3 keV, which were analyzed by a similar SEM (JSM-6360LV, JEOL)-EDS (JED2201, JEOL) system (Oyabu, 2015; Oyabu and others, 2015). Because their method excluded the signals from the surrounding ice and air-hydrate crystals, and their findings being consistent with ours, we argue that the fine particles associated with the air-hydrate crystals analyzed in this study contain almost no elements showing Ar peaks. The Ar is thus most likely from the air-hydrate crystal.

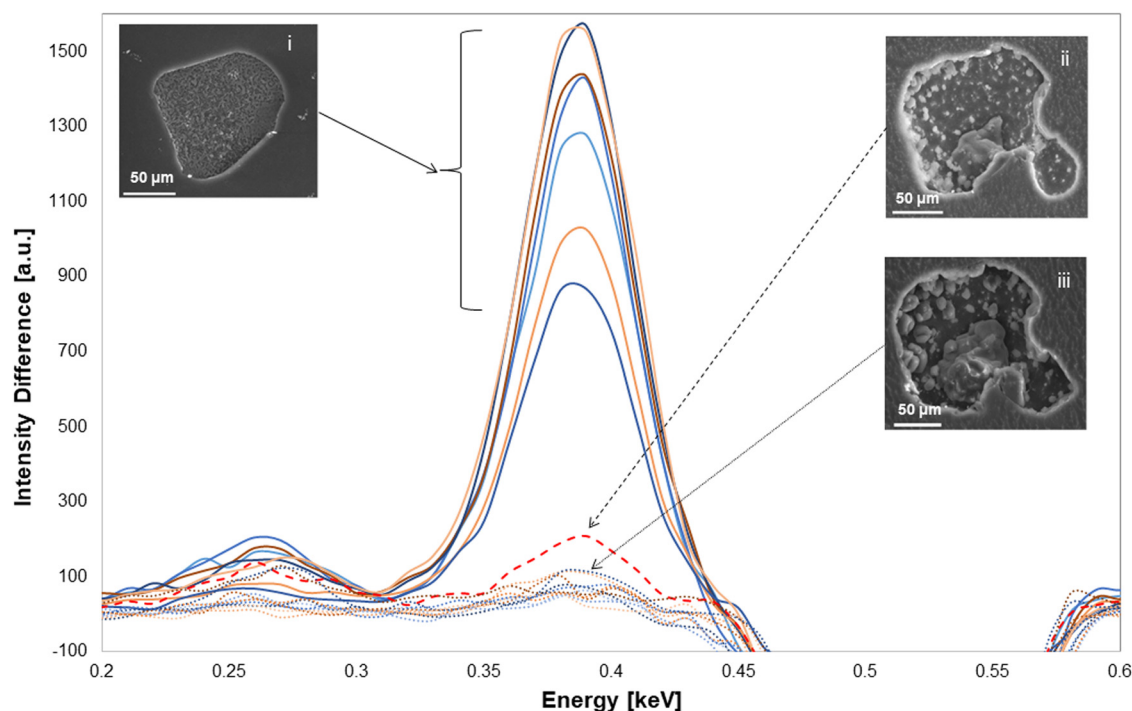


Fig. 10. Differential spectra of N-peak (~ 0.39 keV) intensity of H5 (inset images) after succession of sublimation steps. Images are from the temperature–time series in Figure 5.

4. Conclusions

In this study, we ran SEM-EDS measurements on air-hydrate crystals from sections at 1548 m and 2406 m of the NEEM ice core, Greenland. The measurements gave direct experimental evidence of enclathrated Ar in five air-hydrate crystals below the bubble-air-hydrate crystal transition zone. The difference EDS spectrum between air-hydrate crystal and surrounding ice had an N peak, thus indicating the existence of N_2 in the air-hydrate crystals. Although N_2 in the air-hydrate crystal had been detected before by Raman spectroscopy, it had not been detected with EDS. These results showed that the SEM-EDS measurement is a promising method for observing the presence of Raman-inactive inert gases in air-hydrate crystals. Future studies with this method will examine the composition ratios of the components in the air-hydrate crystals.

Supplementary material. The supplementary material for this article can be found at <https://doi.org/10.1017/jog.2021.115>.

Acknowledgements. We thank all the NEEM project members involved in logistics, drilling, and ice core processing. NEEM is directed and organized by the Centre of Ice and Climate at the Niels Bohr Institute and the United States National Science Foundation, Office of Polar Programs. NEEM is supported by funding agencies and institutions in Belgium (FNRS-CFB and FWO), Canada (NRCan/GSC), China (CAS), Denmark (FIST), France (IPEV, CNRS/INSU, CEA, and ANR), Germany (AWI), Iceland (RannIs), Japan (NIPR), Korea (KOPRI), The Netherlands (NWO/ALW), Sweden (VR), Switzerland (SNF), the United Kingdom (NERC), and the USA (US NSF, Office of Polar Programs).

This study was supported by the Environment Research and Technology Development Fund (JPMERF20202003) of the Environmental Restoration and Conservation Agency of Japan, the Japan Society for the Promotion of Science KAKENHI (Grants JP22221002, JP18H04140, JP20H04327 and JP20H04980), the Arctic Challenge for Sustainability (ArCS) project (JPMXD1300000000), the Arctic Challenge for Sustainability II (ArCS II) project (JPMXD1420318865), a grant for the National Institute of Polar Research, Japan (Project Research KP305 and General Collaboration Project no. 3-6), and the Graduate University for Advanced Studies, SOKENDAI.

We acknowledge Professor Nobuhiko Azuma and Dr Morimasa Takata

(Nagaoka University of Technology) for their technical supports and fruitful discussion. We would also like to thank Dr Jon Nelson (Redmond Phys. Sci.) for English language editing, anonymous reviewers and the scientific editor for their reviewing and editorial comments.

References

- Barnes PRF, Mulvaney R, Robinson K and Wolff EW (2002) Observation of polar ice from the Holocene and the glacial period using the scanning electron microscope. *Annals of Glaciology* **35**, 539–566. doi: [10.3189/172756402781816735](https://doi.org/10.3189/172756402781816735)
- Barnola JM, Raynaud D, Korotkevich YS and Lorius C (1988) Vostok ice core provides 160,000-year record of atmospheric CO_2 . *Nature* **329**, 408–414. doi: [10.1038/329408a0](https://doi.org/10.1038/329408a0)
- Bazin L, Landais A, Lemieux-Dudon B, Toyé Mahamadou Kele H and Veres D and 17 others (2013) An optimized multi-proxy, multi-site Antarctic ice and gas orbital chronology (AICC2012): 120–800 ka. *Climate of the Past* **9**, 1715–1731. doi: [10.5194/cp-9-1715-2013](https://doi.org/10.5194/cp-9-1715-2013)
- Bazin L, Landais A, Capron E, Masson-Delmotte V and Ritz C and 5 others (2016) Phase relationships between orbital forcing and the composition of air trapped in Antarctic ice cores. *Climate of the Past* **12**, 729–748. doi: [10.5194/cp-12-729-2016](https://doi.org/10.5194/cp-12-729-2016)
- Bender ML (2002) Orbital tuning chronology for the Vostok climate record supported by trapped gas composition. *Earth and Planetary Science Letters* **204**, 275–289. doi: [10.1016/S0012-821X\(02\)00980-9](https://doi.org/10.1016/S0012-821X(02)00980-9)
- Bender M, Sowers T and Lipenkov V (1995) On the concentrations of O_2 , N_2 , and Ar in trapped gases from ice cores. *Journal of Geophysical Research: Atmospheres* **100**(D9), 18651. doi: [10.1029/94jd02212](https://doi.org/10.1029/94jd02212)
- Bender ML, Barnett B, Dreyfus G, Jouzel J and Porcelli D (2008) The contemporary degassing rate of ^{40}Ar from the solid earth. *Proceedings of the National Academy of Sciences of the United States of America* **105**(24), 8232–8237. doi: [10.1073/pnas.0711679105](https://doi.org/10.1073/pnas.0711679105)
- Bereiter B, Shackleton S, Baggenstos D, Kawamura K and Severinghaus J (2018) Mean global ocean temperatures during the last glacial transition. *Nature* **553**, 39–44. doi: [10.1038/nature25152](https://doi.org/10.1038/nature25152)
- Chappellaz J, Stowasser C, Blunier T, Baslev-Clausen D and Brook EJ and 8 others (2013) High-resolution glacial and deglacial record of atmospheric methane by continuous-flow and laser spectrometer analysis along the NEEM ice core. *Climate of the Past* **9**, 2579–2593. doi: [10.5194/cp-9-2579-2013](https://doi.org/10.5194/cp-9-2579-2013)

- Davidson DW, Handa YP, Ratcliffe CI, Tse JS and Powell BM (1984) The ability of small molecules to form clathrate hydrates of structure II. *Nature* **311**, 143–143. doi: [10.1038/311142a0](https://doi.org/10.1038/311142a0)
- Eichler J, Kleitz I, Bayer-Giraldi M, Jansen D and Kipfstuhl S and 3 others (2017) Location and distribution of micro-inclusions in the EDML and NEEM ice cores using optical microscopy and in situ Raman spectroscopy. *The Cryosphere* **11**, 1075–1090. doi: [10.5194/tc-11-1075-2017](https://doi.org/10.5194/tc-11-1075-2017)
- Fujita S, Okuyama J, Hori A and Hondoh T (2009) Metamorphism of stratified firn at Dome Fuji, Antarctica: a mechanism for local insolation modulation of gas transport conditions during bubble close off. *Journal of Geophysical Research* **114**, F03023. doi: [10.1029/2008JF001143](https://doi.org/10.1029/2008JF001143)
- Goldstein JI, Newbury DE, Echlin P, Joy DC and Lyman CE and 3 others (2003) *Scanning Electron Microscopy and X-ray Microanalysis*. 3rd Edn. Boston, US: Springer. ISBN: 978-1-4615-0215-9.
- Hondoh T and 5 others (1990) The crystallographic structure of the natural air-hydrate in Greenland Dye-3 deep ice core. *Journal of Inclusion Phenomena and Molecular Recognition in Chemistry* **8**(1–2), 17–24. doi: [10.1007/BF01131284](https://doi.org/10.1007/BF01131284)
- Huber C, Beyerle U, Leuenberger M, Schwander J and Kipfer R and 3 others (2006) Evidence for molecular size-dependent gas fractionation in firn air derived from noble gases, oxygen, and nitrogen measurements. *Earth and Planetary Science Letters* **243**, 61–73. doi: [10.1016/j.epsl.2005.12.036](https://doi.org/10.1016/j.epsl.2005.12.036)
- Ikeda T, Fukazawa H, Mae S, Pepin L and Duval P and 3 others (1999) Extreme fractionation of gases caused by formation of clathrate hydrates in Vostok Antarctic ice. *Geophysical Research Letters* **26**, 91–94. doi: [10.1029/1998GL900220](https://doi.org/10.1029/1998GL900220)
- Ikeda-Fukazawa T, Hondoh T, Fukumura T, Fukazawa H and Mae S (2001) Variation in N₂/O₂ ratio of occluded air in Dome Fuji Antarctic ice. *Journal of Geophysical Research* **106**, 17799–17810. doi: [10.1029/2000JD000104](https://doi.org/10.1029/2000JD000104)
- Ikeda-Fukazawa T, Kawamura K and Hondoh T (2004) Diffusion of nitrogen gas in ice Ih. *Chemical Physics Letters* **385**(5–6), 467–471. doi: [10.1016/j.cplett.2004.01.021](https://doi.org/10.1016/j.cplett.2004.01.021)
- Ikeda-Fukazawa T and 5 others (2005) Effects of molecular diffusion on trapped gas composition in polar ice cores. *Earth and Planetary Science Letters* **229**, 183–192. doi: [10.1016/j.epsl.2004.11.011](https://doi.org/10.1016/j.epsl.2004.11.011)
- Kawamura K, Parrenin F, Lisiecki L, Uemura R and Vimeux F and 13 others (2007) Northern hemisphere forcing of climatic cycles in Antarctica over the past 360,000 years. *Nature* **448**, 912–916. doi: [10.1038/nature06015](https://doi.org/10.1038/nature06015)
- Kobashi T, Severinghaus JP, Brook EJ, Barnola J-M and Grachev AM (2007) Precise timing and characterization of abrupt climate change 8200 years ago from air trapped in polar ice. *Quaternary Science Reviews* **26**(9–10), 1212–1222. doi: [10.1016/j.quascirev.2007.01.009](https://doi.org/10.1016/j.quascirev.2007.01.009)
- Kobashi T, Severinghaus JP and Barnola J-M (2008a) 4 ± 1.5°C Abrupt warming 11,270 yr ago identified from trapped air in Greenland ice. *Earth and Planetary Science Letters* **268**(3–4), 397–407. doi: [10.1016/j.epsl.2008.01.032](https://doi.org/10.1016/j.epsl.2008.01.032)
- Kobashi T, Severinghaus JP and Kawamura K (2008b) Argon and nitrogen isotopes of trapped air in the GISP2 ice core during the Holocene epoch (0–11,500 B.P.): methodology and implications for gas loss processes. *Geochimica et Cosmochimica Acta* **72**(1), 4675–4686. doi: [10.1016/j.gca.2008.07.006](https://doi.org/10.1016/j.gca.2008.07.006)
- Kobashi T, Ikeda-Fukazawa T, Suwa M, Schwander J and Kameda T and 4 others (2015) Post bubble-closeoff fractionation of gases in polar firn and ice cores: effects of accumulation rate on permeation through overloading pressure. *Atmospheric Chemistry and Physics Discussions* **15**, 15711–15753. doi: [10.5194/acpt-15-15711-2015](https://doi.org/10.5194/acpt-15-15711-2015)
- Kuhs WF, Genov G, Staykova DK and Hansen T (2004) Ice perfection and onset of anomalous preservation of gas hydrates. *Physical Chemistry Chemical Physics* **6**, 4917–4920. doi: [10.1039/b412866d](https://doi.org/10.1039/b412866d)
- Landais A, Dreyfus G, Capron E, Pol K and Loutre MF and 7 others (2012) Towards orbital dating of the EPICA dome C ice core using δO₂/N₂. *Climate of the Past* **8**, 191–203. doi: [10.5194/cp-8-191-2012](https://doi.org/10.5194/cp-8-191-2012)
- Miller SL (1969) Clathrate hydrates of air in Antarctic ice. *Science (New York, N.Y.)* **165**(3892), 489–490. doi: [10.1126/science.165.3892.489](https://doi.org/10.1126/science.165.3892.489)
- Nagashima HD, Nemoto K and Ohmura R (2018) Phase equilibrium for argon clathrate hydrate at the temperatures from 197.6 K to 274.1 K. *Journal of Chemical Thermodynamics* **127**, 86–91. doi: [10.1016/j.jct.2018.07.019](https://doi.org/10.1016/j.jct.2018.07.019)
- Nakahara J, Shigesato Y, Higashi A, Hondoh T and Langway CC Jr (1988) Raman spectra of natural clathrates in deep ice cores. *Philosophical Magazine B* **57**, 421–430. doi: [10.1080/13642818808208514](https://doi.org/10.1080/13642818808208514)
- NEEM community members (2013) Eemian interglacial reconstructed from a Greenland folded ice core. *Nature* **493**, 489–494. doi: [10.1038/nature11789](https://doi.org/10.1038/nature11789)
- Ohno H, Lipenkov VYa and Hondoh T (2010) Formation of air clathrate hydrates in polar ice sheets: heterogeneous nucleation induced by micro-inclusions. *Journal of Glaciology* **56**, 917–921. doi: [10.3189/002214310794457317](https://doi.org/10.3189/002214310794457317)
- Orsi AJ, Cornuelle BD and Severinghaus JP (2014) Magnitude and temporal evolution of Dansgaard-Oeschger event 8 abrupt temperature change inferred from nitrogen and argon isotopes in GISP2 ice using a new least-squares inversion. *Earth and Planetary Science Letters* **395**(C), 81–90. doi: [10.1016/j.epsl.2014.03.030](https://doi.org/10.1016/j.epsl.2014.03.030)
- Orsi AJ, Kawamura K, Masson-Delmotte V, Fettweis X and Box JE and 4 others (2017) The recent warming trend in North Greenland. *Geophysical Research Letters* **44** (12), 6235–6243. doi: [10.1002/2016GL072212](https://doi.org/10.1002/2016GL072212)
- Oyabu I (2015) Chemical compositions of past soluble aerosols reconstructed from Greenland and Antarctic ice cores. Ph.D thesis, Hokkaido University. doi: [10.14943/doctoral.k11789](https://doi.org/10.14943/doctoral.k11789)
- Oyabu I, Iizuka Y, Fischer H, Schüpbach S and Gfeller G and 4 others (2015) Chemical compositions of solid particles present in the Greenland NEEM ice core over the last 110,000 years. *Journal of Geophysical Research – Atmospheres* **120** (18), 9789–9813. doi: [10.1002/2015jd023290](https://doi.org/10.1002/2015jd023290)
- Oyabu I, Kawamura K, Kitamura K, Dallmayr R and Kitamura A and 10 others (2020) New technique for high-precision, simultaneous measurements of CH₄, N₂O and CO₂ concentrations, isotopic and elemental ratios of N₂, O₂ and Ar, and total air content in ice cores by wet extraction. *Atmospheric Measurement Techniques* **13**, 6703–6731. doi: [10.5194/amt-13-6703-2020](https://doi.org/10.5194/amt-13-6703-2020)
- Oyabu I, Kawamura K, Uchida T, Fujita S and Kitamura K and 6 others (in review, 2021). Fractionation of O₂/N₂ and Ar/N₂ in the Antarctic ice sheet during bubble formation and bubble-clathrate hydrate transition from precise gas measurements of the dome Fuji ice core. *The Cryosphere*. doi: [10.5194/tc-2021-147](https://doi.org/10.5194/tc-2021-147)
- Rasmussen SO, Abbott PM, Blunier T, Bourne AJ and Brook E and 19 others (2013) A first chronology for the North Greenland Eemian Ice Drilling (NEEM) ice core. *Climate of the Past* **9**, 2713–2730. doi: [10.5194/cp-9-2713-2013](https://doi.org/10.5194/cp-9-2713-2013)
- Safety Data Sheet of Tissue Tek: <https://www.sakura-finetek.com/ja/customer-support/safety-data-sheets> (last visited on April, 2, 2021).
- Salamatin AN, Lipenkov VYa, Ikeda-Fukazawa T and Hondoh T (2001) Kinetics of air-hydrate nucleation in polar ice sheets. *Journal of Crystal Growth* **223**, 285–305. doi: [10.1016/S0022-0248\(00\)01002-2](https://doi.org/10.1016/S0022-0248(00)01002-2)
- Salamatin AN, Lipenkov VYa and Hondoh T (2003) Air-hydrate crystal growth in polar ice. *Journal of Crystal Growth* **257**, 412–426. doi: [10.1016/S0022-0248\(03\)01472-6](https://doi.org/10.1016/S0022-0248(03)01472-6)
- Satoh K, Uchida T, Hondoh T and Mae S (1996) Diffusion coefficient and solubility measurements of noble gases in ice crystals. *Proceedings of the NIPR Symposium on Polar Meteorology and Glaciology* **10**, 73–81.
- Schüpbach S, Fischer H, Bigler M, Erhardt T and Gfeller G and 46 others (2018) Greenland records of aerosol source and atmospheric lifetime changes from the Eemian to the Holocene. *Nature Communications* **9** (1), 1476. doi: [10.1038/s41467-018-03924-3](https://doi.org/10.1038/s41467-018-03924-3)
- Severinghaus JP (1999) Abrupt climate change at the end of the Last Glacial Period inferred from trapped air in polar ice. *Science (New York, N.Y.)* **286** (5441), 930–934. doi: [10.1126/science.286.5441.930](https://doi.org/10.1126/science.286.5441.930)
- Severinghaus JP and Battle MO (2006) Fractionation of gases in polar ice during bubble close-off: new constraints from firn air Ne, Kr and Xe observations. *Earth and Planetary Science Letters* **243**, 61–73. doi: [10.1016/j.epsl.2005.12.036](https://doi.org/10.1016/j.epsl.2005.12.036)
- Severinghaus JP, Sowers T, Brook EJ, Alley RB and Bender ML (1998) Timing of abrupt climate change at the end of the younger Dryas interval from thermally fractionated gases in polar ice. *Nature Publishing Group* **391**(6663), 141–146. doi: [10.1038/34346](https://doi.org/10.1038/34346)
- Severinghaus JP, Beaudette R, Headly MA, Taylor K and Brook EJ (2009) Oxygen-18 of O₂ records the impact of abrupt climate change on the terrestrial biosphere. *Science (New York, N.Y.)* **324**(5), 1431–1434. doi: [10.1126/science.1169473](https://doi.org/10.1126/science.1169473)
- Sheldon SG, Steffensen JP, Hansen SB, Popp TJ and Johnsen SJ (2014) The investigation and experience of using ESTISLO™ 240 and COASO™ for ice-core drilling. *Annals of Glaciology* **55**(68), 219–232. doi: [10.3189/2014AoG68A036](https://doi.org/10.3189/2014AoG68A036)

- Shigeyama W, Nagatsuka N, Homma T, Takata M and Goto-Azuma K and 7 others** (2019) Microstructural analysis of Greenland ice using a cryogenic scanning electron microscope equipped with an electron backscatter diffraction detector. *Bulletin of Glaciological Research* **37**, 31–45. doi: [10.5331/BGR.19R01](https://doi.org/10.5331/BGR.19R01)
- Shigeyama W, Nakazawa F, Goto-Azuma K, Homma T and Nagatsuka N** (2021) Microparticles in a deep ice core drilled at NEEM, Greenland: cryogenic scanning electron microscopic observations of location, size, shape, and constituent elements. *Polar Data Journal* **5**, 99–124. doi: [10.20575/00000031](https://doi.org/10.20575/00000031).
- Stern LA, Kirby SH, Circone S and Durham WB** (2004) Scanning electron microscopy investigations of laboratory-grown gas clathrate hydrates formed from melting ice and comparison to natural hydrates. *American Mineralogist* **89**(8–9), 1162–1175. doi: [10.2138/am-2004-8-902](https://doi.org/10.2138/am-2004-8-902)
- Suwa M and Bender ML** (2008a) Chronology of the Vostok ice core constrained by O₂/N₂ ratios of occluded air, and its implication for the Vostok climate records. *Quaternary Science Reviews* **27**, 1093–1106. doi: [10.1016/j.quascirev.2008.02.017](https://doi.org/10.1016/j.quascirev.2008.02.017)
- Suwa M and Bender ML** (2008b) O₂/N₂ ratios of occluded air in the GISP2 ice core. *Journal of Geophysical Research – Atmospheres* **113**(11), D11119. doi: [10.1029/2007JD009589](https://doi.org/10.1029/2007JD009589)
- Uchida T and 5 others** (1994a) Brittle zone and air-hydrate formation in polar ice sheets. *Memoirs of National Institute of Polar Research. Special issue* **49**, 312–319.
- Uchida T, Hondoh T, Mae S, Shoji H and Azuma N** (1994b) Optimized storage condition of deep ice core samples from a view point of air-hydrate analysis. *Memoirs of National Institute of Polar Research. Special issue* **49**, 320–327.
- Uchida T, Sakurai T and Hondoh T** (2011) Ice-shielding models for self-preservation of gas hydrates. *Journal of Chemistry and Chemical Engineering* **5**(8), 691–705.
- Uchida T, Yasuda K, Oto Y, Shen R and Ohmura R** (2014) Natural supersaturation conditions needed for nucleation of air clathrate hydrates in deep ice sheets. *Journal of Glaciology* **60**(224), 1111–1116. doi: [10.3189/2014JoG13J232](https://doi.org/10.3189/2014JoG13J232)